First publ. in: Surface Science 604 (2010), 3-4, pp. 269-275

Electronic structure of thin ytterbium layers on W(1 1 0): A photoemission study

Yu.S. Dedkov [a,b,*], D.V. Vyalikh [a], M. Weser [a], M. Holder [a], S.L. Molodtsov [a], C. Laubschat [a], Yu. Kucherenko [c], M. Fonin [d]

[a] Institut für Festkörperphysik, Technische Universität Dresden, 01062 Dresden, Germany
[b] Fritz-Haber Institut der Max-Planck Gesellschaft, 14195 Berlin, Germany
[c] Institute for Metal Physics, National Academy of Sciences of Ukraine, 03142 Kiev, Ukraine
[d] Fachbereich Physik, Universität Konstanz, 78457 Konstanz, Germany

A B S T R A C T

In the present work we report on high-quality results of angle-resolved photoemission studies of thin Yb layers (1–3 ML thick) on a W(1 1 0) substrate. Growth of the thin Yb layers was monitored via permanent measurements of photoemission spectra during Yb deposition. This method allows to monitor the thickness of the deposited Yb with very high accuracy due to strong layer-dependent binding energy shifts of the Yb 4*f* emission. Contrasting to Ce/W(1 1 0) no hybridization of the 4*f* states with the own 6*s*-derived band is observed for the Yb layers. Instead, a splitting of the Yb $4f_{7/2}$ emission is observed around the Γ-point that is due to interactions with the W 5*d*-derived substrate band and could quantitatively be described in the framework of the Periodic Anderson model.

Keywords:
Ytterbium
Photoelectron spectroscopy
Thin films
Anderson model

1. Introduction

In recent years, investigations of Kondo-like phenomena in Ce and Yb systems have attracted considerable interest. Both elements form compounds with either magnetic or non-magnetic, mixed-valent and heavy-Fermion-like properties. In analogy to the famous $\alpha \rightarrow \gamma$ transition of Ce metal that was assigned to a Kondo-collapse a respective phase transition has also been reported for Yb metal [1]. The analogy of these two elements has been explained on the basis of the electron-hole symmetry of the quasiatomic 4*f* shell [2,3]. This symmetry, however, is broken by the fact that the 4*f* occupancy of Ce is always close to 1 for metallic systems, while the number of 4*f* holes in Yb may assume any value between 1 and 0 and is particularly close to zero in divalent Yb metal. This different behavior may be understood in the framework of the single-impurity Anderson model (SIAM), where the 4*f* occupancy depends on the binding energy of the unhybridized $4f^n$ configurations, ε and a hybridization parameter, Δ, that describes the electron hopping probability between 4*f* and valence band (VB) derived states. In case of Ce the unhybridized trivalent $4f^1$ ground state corresponds to an ε value of about -2 eV in the pure metal and increases to about -1 eV in transition metal compounds, while Δ is large and varies strongly with composition describing interactions of the rather extended 4*f* states with the surrounding valence bands. In case of Yb, on the other hand, the increased nuclear charge leads to a stronger localization of the 4*f* orbitals as reflected by a much smaller Δ as compared to respective Ce systems, while the divalent ground state of Yb metal corresponds to a positive ε value of the unhybridized hole state of about 0.5 eV that, however, may change its sign by means of thermochemical effects in compounds. Consequently, in Ce systems changes of the electronic properties are mainly driven by variations of the matrix elements, while in Yb systems they are governed by the binding energy of the unhybridized $4f^{13}$ state. Values for the parameters ε and Δ may be obtained from 4*f* photoemission (PE) spectra that in case of Ce have a characteristic double-peak structure, a "ionization" peak ($4f^0$ final-state) at a binding energy (BE) of $\sim \sqrt{\varepsilon^2 + 4\Delta^2}$ and a "hybridization" (or Kondo) peak ($4f^1$ final-state) at the Fermi energy, E_F, with a relative intensity of $\sim (\Delta/\varepsilon)^2$ with respect to the former. For divalent Yb systems the situation is more difficult, since due to small Δ the PE spectra reveal only a strong $4f^{13}$ final-state doublet at a BE of $\sim |\varepsilon|$ and only for small ε (mixed-valence limit) appearance of an additional $4f^{12}$ final-state multiplet at about 5 eV BE allows for direct estimation of Δ.

Both metals, Ce and Yb, may be grown as structurally ordered films on W(1 1 0) forming an incoherent interface between the *fcc* (1 1 1) face of the rare earth (RE) overlayer and the *bcc* (1 1 0) surface of the tungsten substrate. For a Ce monolayer (ML) on W(1 1 0) the interatomic distances between neighboring Ce atoms are even smaller than in α-Ce metal leading to a strongly hybridized behavior reflected in the PE spectra by a large hybridization

* Corresponding author. Address: Fritz-Haber Institut der Max-Planck Gesellschaft, Faradayweg 4-6, 14195 Berlin, Germany. Tel.: +49 30 84135628.
E-mail address: dedkov@fhi-berlin.mpg.de (Yu.S. Dedkov).

peak and a splitting of the ionization peak around the point in k-space where the unhybridized $4f^0$ state coincides in energy with the Ce 6s-derived band [4]. This phenomenon could be explained in the framework of the periodic Anderson model (PAM) [5–7]. A simple approach to this model [8] explains obtained results by the formation of symmetric and antisymmetric linear combinations of 6s and 4f states separated from each other by a hybridization gap of the order of 2Δ.

In case of a Yb monolayer on W(1 1 0) no deviation of the lattice constant with respect to Yb metal has been reported. However, since the decrease of the lattice constant in the stronger hybridized low-temperature phase amounts to only 4% with respect to α-Yb a respective effect in the Yb monolayer may be below the resolution of a low-energy electron diffraction (LEED) experiment. On the other hand, as in the case of a Ce monolayer one might expect energy splittings of the 4f states in those regions of **k**-space, where energy degeneracies of 4f and Yb 6s states take place. In fact, **k**-dependent splittings of the Yb 4f emission have been reported for Yb-based heavy-fermion compounds [9], and observation of a similar effect for the Yb monolayer could allow for determination of Δ.

In the present paper we report on an angle-resolved PE study of thin Yb films on W(1 1 0). The 4f emission reveals strong layer-dependent BE shifts, that may be understood quantitatively in the framework of a hypothetical Born–Haber cycle and allow for a proper discrimination of mono-, double- and three-layer coverages. No energy gap formation is observed around the energy crossing of the 4f states with the Yb 6s-derived band what is ascribed to stronger localization of both the 4f and 6s states in Yb as compared to Ce metal. On the other hand, a splitting of the $4f_{7/2}$ state is observed around the $\bar{\Gamma}$-point of the surface Brillouin zone (SBZ) where the 4f state is energetically degenerate with a bunch of W 5d-derived bands. From the fact that this phenomenon is not observed at other **k** points one can conclude that the effect is not related to an interaction of the incoherent lattices but reflects a **k**-dependent interaction of Yb impurities with W-derived bands.

2. Experimental details

Photoemission experiments were performed at U49/2-PGM-1 undulator beamline of BESSY (Berlin). PE spectra were acquired with a hemispherical electron energy analyzer during deposition of Yb metal at very low deposition rates from a carefully degassed and shielded evaporation source (e-beam heated W-crucible) (see Fig. 1a for the scheme of experiment). The overall-system energy resolution was set to 100 meV (FWHM) and an angular resolution better than 1° was used. Structurally ordered layers of Yb metal were grown on a W(1 1 0) substrate kept at room temperature. Prior to Yb deposition, the W(1 1 0) substrate was carefully cleaned by repeated cycles of heating up to 1300 °C in oxygen ambient pressure of 5×10^{-8} mbar for 15 min and subsequent flashing up to 2300 °C. Samples prepared in this way exhibit a high crystalline quality as monitored by low-energy electron diffraction (LEED). The thickness of the deposited Yb layers was simultaneously monitored with a calibrated quartz oscillator. All PE spectra were taken at $h\nu = 110$ eV in order to increase the photoelectron emission from Yb 4f states considerably and suppress that from 5d states of tungsten that are close to a Cooper minimum of the photoionization cross section at this photon energy (Fig. 1b). The base pressure in the experimental chamber was below than 5×10^{-11} mbar rising to 1×10^{-10} mbar during metal evaporation as monitored by the absence of any oxygen trace in the spectra.

3. Results and discussions

3.1. Thickness dependence of the Yb 4f signal

Fig. 2 shows a series of PE spectra taken at 110 eV photon energy for different Yb coverages of the W(1 1 0) substrate and normalized to equal maximal intensity. An emission angle 5° off-normal was chosen in order to eliminate effects that appear close to normal emission and will be discussed later. At the bottom, the spectrum of the pure W(1 1 0) substrate is shown characterized

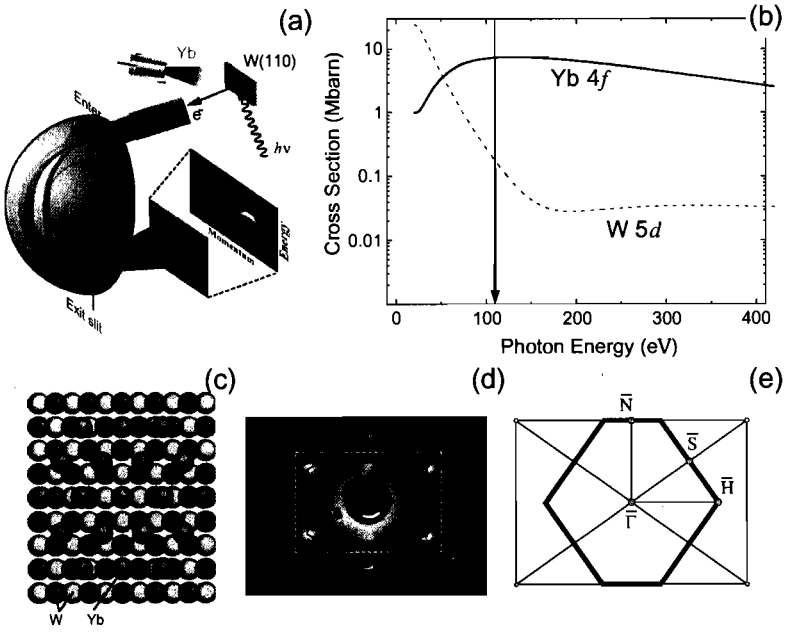

Fig. 1. (a) Scheme of the PE experiment on Yb/W(110) systems. (b) Photoionization cross section for the Yb 4f and W 5d shells. The photon energy used in the present experiment is 110 eV and marked by an arrow in the plot. (c) Arrangement of the Yb monolayer on W(1 1 0). (d) LEED image of a Yb monolayer on W(1 1 0). The corresponding lattices of Yb and W in reciprocal space are marked by solid and dashed lines, respectively. (e) Brillouin zone of the W(1 1 0) surface with some high symmetry points.

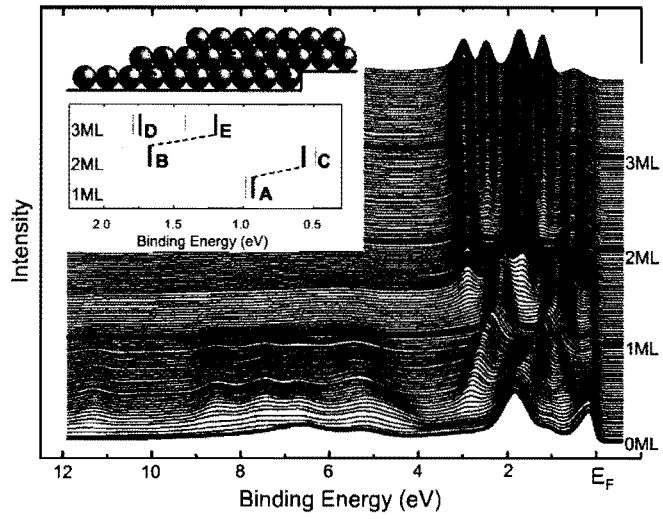

Fig. 2. Photoemission spectra obtained during continuous Yb deposition on W(1 1 0) surface. The inset shows the energy positions of the Yb $4f_{7/2}$ line for Yb coverages of 1, 2 and 3 ML: thick lines – experimental data, thin lines – calculated data on the basis of Slater's transition state concept.

by a d_{z^2}-like surface state at E_F, strong emissions from W 5*d*-derived volume bands around 1.9 eV binding energy and mostly W 6*s*-derived features between 5 and 7 eV BE [10]. Deposition of small amounts of Yb on top of the W(1 1 0) surface leads to the appearance of strong Yb 4*f* emissions, consisting of a $4f^{13}$ doublet at 1.6 and 2.8 eV BE and a broad $4f^{12}$ final state multiplet [11] between 4 and 9 eV BE, respectively. Since the $4f^{13}$ doublet is found far below the Fermi energy it is not likely to ascribe the appearance of two different final-state configurations to a mixed-valent ground state but to coexistence of di- and trivalent Yb atoms at the surface. The trivalent state is hereby ascribed to highly coordinated Yb atoms at steps of the W substrate (atom's position "S" in the inset of Fig. 2) while for low coordinated Yb atoms at terrace sites a divalent configuration is expected (atom's position "A") [12,13]. As expected, the intensity of the trivalent component remains, therefore, constant upon further Yb deposition while the intensity of the divalent component increases linearly with coverage (note that the seeming decrease of the trivalent component with coverage is an artifact caused by the normalization of the spectra). Parallel to the intensity increase of the divalent component, the BE of the $4f^{13}_{7/2}$ line decreases linearly from 1.6 to 0.91 eV, and at the same time the spin-orbit splitting increases from 1.22 to 1.28 eV. The variations of the 4*f* BE may be related to changes in the effective Yb–Yb coordination [14]: For low Yb coverages charge transfer from Yb to the W substrate may be expected according to the different electronegativities of Yb and W leading to a positive charging of the adsorbed atoms. Charging leads to a repulsive interaction between the adsorbed atoms that prevents island formation and induces an homogeneous distribution of the ions on the surface. With increasing coverage the density of adsorbed atoms increases, the charge transfer reduces due to corroborative interactions of the ions, and finally a metallic Yb overlayer is formed. In this picture the variations of binding energy reflect both decreasing ionicity of the Yb atoms and increasing valence band width with coverage that leads to a respective increase of cohesive energy. The linearity of the effect and the fact that the emission lines are rather sharp and do not change their width as a function of coverage support the assumption that island growth is inhibited: Inequivalent adsorption sites at the border or within the islands should be reflected by a simultaneous appearance of 4*f* components at different binding energies [14]. Variations of the spin-orbit splitting of adsorbate have been reported for the Cs 5*p* core level spectra of submonolayers of Cs on Si(1 1 1) [15]. There, the effect was explained by a decrease of the gradient of the core-potential caused by screening due to the surface state of Si. In analogy to this observation changes of 4*f* multiplet splittings observed in Bremsstrahlung-isochromate spectra of several RE intermetallics were related by the same arguments to the local electron density [16]. In the present case similar arguments may be applied to the observed variation of the spin-orbit splitting since the assumed positive charging of the Yb atoms is not necessarily in contradiction to a change of the gradient of the core-potential caused by screening due to the W surface state. On the other hand, hybridization of the 4*f* final-state with the W 5*d* derived valence band could be an alternative explanation as is discussed in more detail below.

Exceeding a coverage of 1 ML two additional $4f^{13}_{7/2}$ components appear at 1.65 eV ("B") and 0.54 eV ("C") BE (see Fig. 2) that both grow in intensity with increasing coverage while the intensity of component "A" decreases and disappears when the 2nd layer is completed. While component "A" arises from a monolayer Yb on W, component "B" is attributed to Yb atoms in the second layer, and component "C" is interpreted as interface component caused by Yb atoms of the first layer that are covered by surface atoms of the second layer [12]. Exceeding a coverage of 2 ML, component "B" converts into component "D" at 1.73 eV and a new component "E" appears at 1.21 eV, that correspond in their binding energies to emissions from Yb atoms at close-packed surfaces and bulk Yb metal. With increasing intensity of component "E", components "B" and "C" decrease in intensity leading to the conclusion, that component "E" stems from Yb atoms of the second layer that are covered by surface atoms of the third layer.

Components "B", "C", "D" and "E" have been observed previously at almost the same BEs for the isoelectronic system Yb/Mo(1 1 0) [12]. The energy positions of surface and bulk emissions of Yb metal (components "D" and "E", respectively) are well described by means of a hypothetical Born–Haber cycle [17] replacing the fully-screened PE final state by a trivalent Yb atom dissolved in the matrix of divalent Yb metal. The respective Born–Haber cycle consists of evaporation of the divalent metal, photoionization in the gas phase, neutralizing the photoion by an additional valence electron, condensation of the trivalent atoms to a solid and dissolution of this trivalent solid in the divalent metal. As a result, the bulk BE deviates from the BE in a free atom

essentially by the difference in cohesive energy in the divalent and trivalent phase, and the surface energy shift could be explained by considering the coordination dependence of the cohesive energies within a tight-binding model [14]. Within the same approach the authors of Ref. [12] were able to relate the energy position of the interface component "C" with respect to components "B" and "E" to the adhesion and segregation energies of the Yb/Mo system, respectively. Calculations of the respective quantities by means of the semi-empirical Miedema's scheme [18] lead to perfect agreement of theory and experiment.

Component "A" was not discussed before since the studies reported in [12] were restricted to coverages larger than two monolayers. Using similar arguments as the authors of Ref. [12] we will show in the following that the energy shift between components "A" and "C" equals to the surface energy shift between components "D" and "E". In order to illustrate our thermochemical arguments we use in Fig. 3 the same type of diagrams as introduced in Ref. [12]. With line (a) in Fig. 3 we consider the energy necessary to cut an Yb crystal along a (1 1 1) lattice plane, that should be almost the same whether a pure Yb crystal is considered (left hand side of the line (a)) or the cut is performed between the first and second Yb layer of a Yb/W-system [right hand side of line (a) in Fig. 3] since the same number of bonds between Yb atoms are broken. An analogous argument holds for the case that a Yb crystal with a trivalent impurity is considered (Fig. 3, line (b)). Again, the energy necessary to cut the crystal leaving the impurity in the surface plane should be almost independent from the fact, whether the Yb crystal below the surface layer is replaced by W or not (compare Fig. 3, line (a)). Considering now the difference between lines (a) and (b), the contributions of the cut Yb crystals on the right hand side of the brackets cancel each other, and as a result we find on both sides of the equation differences of brackets that describe each the energy necessary to replace a divalent atom at a specific site by a trivalent one. Adding now to each bracket the $f \rightarrow d$ excitation energy necessary to convert a divalent Yb atom into a trivalent one, the brackets may be replaced by respective PE binding energies and we obtain: $E_B(\text{bulk}) - E_B(\text{surf}) = E_B(\text{interf}) - E_B(\text{ML})$. Thus, the BE shift between components "C" and "A", $E_B(\text{interf}) - E_B(\text{ML})$ equals the surface energy shift of the 4*f* states. Introducing the experimental numbers we find that in reality the BE shift of components "C" and "A" (0.37 eV) is somewhat smaller than the shift between components "E" and "D" (0.52 eV). On the other hand, the latter value is larger than the surface energy shift reported for Yb atoms with coordination 9 (0.45 eV [19]) indicating that in the present case the surface layer contains many atoms at lower coordinated sites and is, thus, still not completed. Applying similar arguments to the Yb monolayer, one may conclude that the 4*f* binding energy for an ideal monolayer is somewhat smaller than the experimentally observed value of component "A", leading to an increase of the energy shift $E_B(C) - E_B(A)$. Thus, taking these corrections into account the prediction of the thermochemical model are in rather good agreement with the experiment.

Alternatively, layer-dependent BE shifts may be predicted on the basis of the calculated electronic structure of the Yb/W-system. To this end, the atomic structure was simulated by slabs consisting of three atomic layers of W covered by one, two, or three Yb layers. Since the structural periodicity of the Yb/W-system necessary for the simulation is lacking due to the lattice mismatch between Yb(1 1 1) and W(1 1 0) we changed the rectangular structure of W(1 1 0) to a hexagonal one matching them to the Yb(1 1 1) overlayer. In spite of the resulting stretching of the W–W spacings within the layers the interlayer distance between adjacent W-layers was kept constant. The calculations were performed by the linear muffin-tin orbital (LMTO) method [20] treating the fully occupied Yb 4*f* states as localized core levels. Their binding energy was estimated by means of Slater's transition state concept [25] that has been shown to be a good approximation for description of electron transitions within the local-density approximation (LDA) approach. The calculated energy positions of the 4*f*-emissions are shown as thin lines in the inset of Fig. 2 and compared to the experimentally observed binding energies (thick lines). For better comparison with the experiment the calculated values were rigidly shifted by 0.6 eV to higher BE. Such a shift is necessary to account for the effect that in a PE experiment a single divalent Yb atom is converted into a trivalent impurity, while in the simulation the valency of all equivalent atoms within the Yb layer was changed. A respective energy correction was also used in the thermochemical Born–Haber cycle discussed above and can be estimated to be 0.6 eV from the heat of solution of divalent Yb in a trivalent RE metal. As is obvious from the inset of Fig. 2, the agreement between observed and calculated BEs is rather good in spite of the crude approximations used in the computer simulation.

3.2. Hybridization effects in 1 ML Yb/W(1 1 0): experiment

In the following we will concentrate on PE of the Yb monolayer. In the energy region of the $4f^{13}$ final-state multiplet, the valence band of a free-standing two-dimensional Yb layer consists of a free-electron like band mainly derived from Yb 6*s* states. In such a free-standing Yb ML, the bottom of this band is found at 4.3 eV (inset of Fig. 4), shifted with respect to the position of the respective band in Ce by about 1 eV to higher BE [4,26] reflecting the ef-

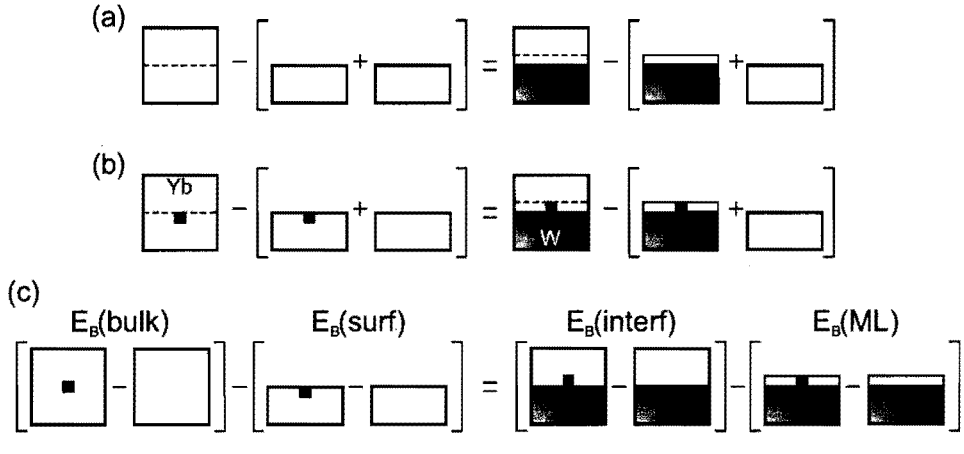

Fig. 3. Illustration of thermochemical calculations used in the manuscript for (a) Yb crystal, (b) Yb crystal with a trivalent impurity and (c) is the difference of (a) and (b).

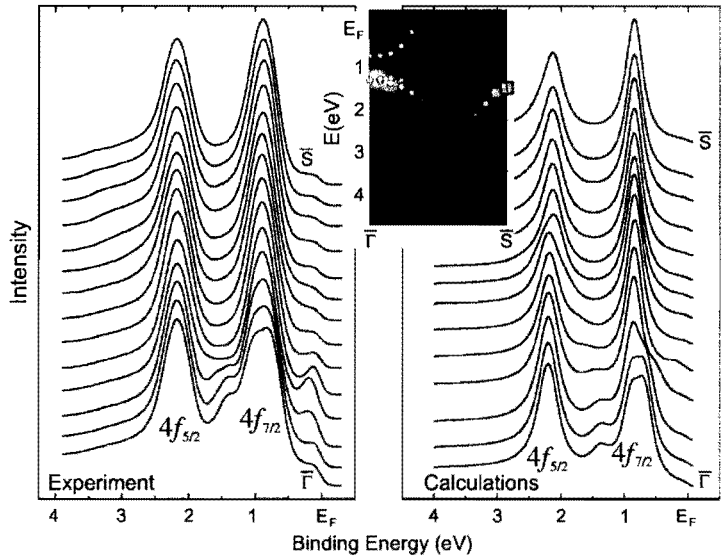

Fig. 4. Experimental (left panel) and theoretically simulated (right panel) angle-resolved photoemission spectra of 1 ML Yb on W(1 1 0). The inset shows experimental angle-resolved photoemission data for W(1 1 0) as color plot measured in $\bar{\Gamma}-\bar{S}$ direction of the SBZ. The size of the symbols in the inset corresponds to the theoretically calculated weight of Yb 5*d* character in the free-standing Yb ML (squares) and the weight of W 5*d* character in valence bands of bulk W (circles).

fect of lanthanide contraction. This band reaches the border of the Brillouin zone at 1.5 eV BE where it gets more Yb 5*d* character. For a two-dimensional overlayer in contact with the W substrate this band may be shifted to lower BE due to charge transfer, in case of Ce this shift amounts to about 1 eV. Assuming a similar shift for the Yb 6*s* derived band one may conclude that probably both 4*f* spin-orbit components, at least the BE position of the $4f_{5/2}$ component, will be crossed by the band. Since the actual **k**-point of the crossing is unknown we show in Fig. 4 (left panel) a series of PE spectra along the $\bar{\Gamma}-\bar{M}$ direction of the surface Brillouin zone including both the $\bar{\Gamma}$ and $\bar{M}$ points (this direction is parallel to the $\bar{\Gamma}-\bar{S}$ direction in the surface Brillouin zone of W(1 1 0) surface). Unfortunately, at 110 eV photon energy the PE cross section of Yb 6*s* states is very low as compared to the one of the 4*f* states and the Yb 6*s* band itself is, therefore, not visible in the PE spectra. However, if there is finite hybridization between the 4*f* states and the 6*s* band this interaction should be reflected by an energy splitting of the 4*f* states as observed for the 4*f* ionization peak in Ce/W(1 1 0) [4]. Careful inspection of the individual 4*f* line shapes shows that within the experimental accuracy limited by energy resolution and natural line-width of the 4*f* final-states only the $4f_{7/2}$ component reveals such an energy splitting around the $\bar{\Gamma}$ point that, however, cannot be related to interactions with the 6*s*-band since the bottom of the latter is expected at much higher BE. Thus, one must conclude that the strength of interaction between the 4*f* states and the 6*s* band is by at least a factor 10 smaller than in the case of Ce. Extrapolating the trends of the hybridization parameters observed for light rare earths in isoelectronic compounds linearly as a function of atomic number, *Z*, to Yb one would expect a reduction of the Δ parameter of about 0.5 of its value in Ce [27]. Thus, the weakness of the interaction in the Yb layer is not so much related to the increased localization of the 4*f* states in the course of lanthanide contraction, but reflects mainly an increased localization of the 6*s* states that leads to weaker 5*d* admixtures to the Bloch-states and to a weaker *f*-character at the Yb site responsible for hybridization with the Yb 4*f* states [4,9].

In order to explain the splitting of the Yb $4f_{7/2}$ component at the $\bar{\Gamma}$-point one might argue that the effect is caused by superposition of the 4*f* line by an underlying residual W emission. To rule out such an interpretation the relative intensity of the $4f_{7/2}$ with respect to the $4f_{5/2}$ component was compared for spectra taken at emission angles of 0° and 7°, respectively. Fig. 5 shows the respective experimental data together with the results of a least-squares fit analysis. The 7° spectrum was described by a pair of Lorentzians, convoluted by a Gaussian to take into account finite experimental resolution and superimposed by an integral background in order to simulate the contributions of inelastically scattered electrons. In case of the 0° spectrum two additional Lorentzians were necessary to yield a good description of the data assuming that all Lorentzians used reveal the same line-width. Comparing now the relative intensity of the $4f_{7/2}$ with respect to the $4f_{5/2}$ component of the 0° spectrum it is evident that at least the two Lorentzians at 0.70 and 1.05 eV must be considered as part of the $4f_{7/2}$ component in order to conserve the intensity ratio observed at the emission angle of 7°. Only the Lorentzian at 1.45 eV may be attributed to residual 5*d*-emissions from the W substrate, that are observed for clean W at the same BE (compare inset of Fig. 4).

3.3. Hybridization effects in 1 ML Yb/W(1 1 0): theory

Similar energy splittings of the Yb $4f_{7/2}$ component have been reported for $YbIr_2Si_2$ [9] and could there quantitatively be described in the framework of a simple approach to PAM. In this approach, the valence band states were described within a LDA band-structure calculation and the unhybridized 4*f* hole ($4f^{13}$ state) was represented by a dispersionless band at energy ε. Like in SIAM, the interaction between valence band and 4*f* states is described by hopping probabilities that depend on the *f*-character of the valence band state at the Yb site, scaled by a hopping parameter, Δ. Neglecting coexistence of two holes at the same Yb site by setting the Coulomb repulsion energy between the holes, U_{ff} to infinite allowed for diagonalization of the Hamiltonian. The result is very similar to the one obtained for SIAM with the only difference that the density of states (DOS) considered in SIAM is now replaced by the energy distribution of states obtained from the band-structure calculation for the respective point in **k**-space.

Applying this approach to the present case of Yb/W is not straightforward, since the incommensurate character of the interface should lead to multiple back-folding and, thus, to a complete smearing of substrate bands in **k**-space. On the other hand, if we

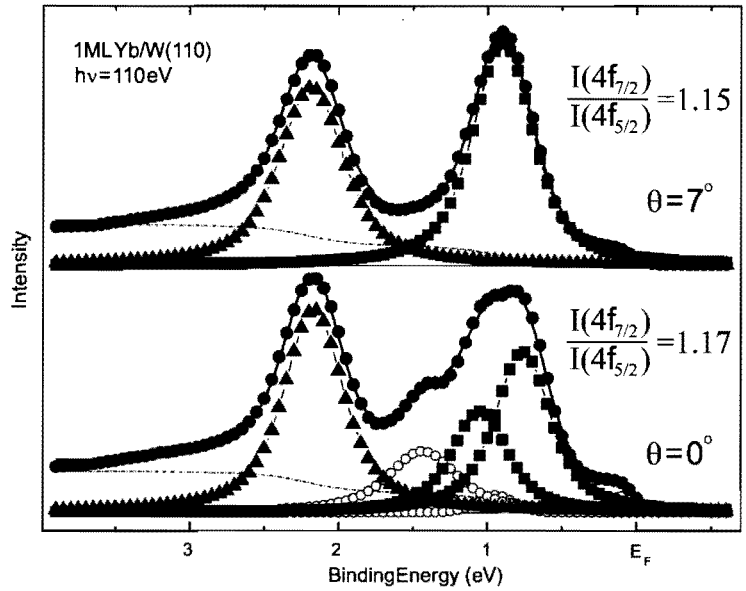

Fig. 5. Results of a least-square fit of experimental photoemission spectra of 1 ML Yb on W(1 1 0) taken at emission angles $\theta = 0°$ and 7°. Emission lines: squares – Yb $4f_{7/2}$, triangles – Yb $4f_{5/2}$, open circles – W 5*d* valence states.

consider the unhybridized Yb 4*f* hole as a localized impurity within the substrate lattice with an spatial extension much smaller than the interatomic W–W distance, then transformation into **k**-space should yield in fact a dispersionless band reflecting the expansion-components of this impurity.

Respective effects have not been observed for Ce/W(1 1 0) [4], possibly because line-width and BE of the Ce $4f^0$ state are much larger than those of the Yb $4f_{7/2}$ component. In order to describe the interaction with the W band in spite of the lattice mismatch in the framework of the PAM one has to consider the Yb $4f^{13}$ hole state as an impurity that interacts predominantly with W 5*d* states directed outward of the W(1 1 0) plane. In order to determine the respective character of the W bands, band-structure calculations have been performed using the linear muffin-tin orbital (LMTO) method [20–24]. The results are shown by white dots in the inset of Fig. 4 where the size of the dots is a measure for the magnitude of the 5*d* admixture to the respective valence band states. The inset also shows experimental angle-resolved PE data for W(1 1 0) measured along the $\bar{\Gamma} - \bar{S}$ direction as a color plot. Strong 5*d* admixtures to the W bands correspond to strong intensities in the PE signal as is expected from the larger cross section of the W 5*d* as compared to the W 6*s* states. The observed variations of the valence band intensities are, thus, in excellent agreement with the expectation based on the band-structure calculations. The interaction with the 4*f* state in the light of PAM may now be handled in a similar way as for the Ce/W(1 1 0) system and the YbX_2Si_2 heavy-fermion compounds: The unhybridized hole state is considered as a dispersionless band at energy $\varepsilon = \varepsilon(\mathbf{k})$ whereby the band character is in the present case not thought to be related to a periodic arrangement of 4*f* states but reflects simply an expansion of an localized impurity state in basis states of the W lattice. The hybridization matrix element is assumed to be proportional to the *d*-projected partial weight of the band states and described by the hybridization parameter, Δ. Using the Anderson formalism in hole representation and excluding double-hole states ($4f^{12}$ configurations) from our consideration by setting the on-site Coulomb correlation energy U_{ff} to infinity allows then for a diagonalization of the Hamiltonian. The obtained result is reminiscent of that of the single-impurity Anderson model (SIAM). The important difference is, however, that now **k** dependence is achieved by replacing the density of states (DOS) used in SIAM by **k**-depending partial weights. Since ε is given by the BE of the $4f_{7/2}$ component at **k** points far away from the $\bar{\Gamma}$ point the proportionality constant Δ (equal to 0.22 eV in accordance with our earlier works on Yb systems) is the only adjustable parameter of this approach.

Fig. 4 (right panel) shows a series of calculated 4*f* spectra along the $\bar{\Gamma} - \bar{S}$ direction of the W(1 1 0) SBZ that reproduces all features observed in the respective experimental data. Note, that particularly the peak at 1.37 eV BE in the normal emission spectrum should not be considered as a pure valence band emission but represents a hybrid state with strong 4*f* admixture. Since in the calculations only the 4*f* character is shown its intensity relative to the unhybridized $4f_{5/2}$ component is weaker than in the experiment. Similar arguments hold for the features close to the Fermi energy that are caused by hybridization of the $4f_{7/2}$ state with an upwards dispersing band. Note, that also for the $4f_{5/2}$ state an intersection with the band is expected from the dispersion. This takes place halfway between the $\bar{\Gamma}$ and $\bar{S}$ points, and in fact the model calculations reveal there a change of the $4f_{5/2}$ line shape. This change, however, is very weak because the *d* admixture to the valence band state is small and this effect is beyond the experimental resolution.

4. Conclusion

In summary, the observed layer-depended shifts observed for Yb/W(1 1 0) are in good agreement with thermochemical predictions based on a hypothetical Born–Haber cycle. Contrasting to the case of Ce/W(1 1 0), no interactions of the 4*f* states with 6*s*-derived bands are observed for the Yb monolayer. This is not so much related to an increasing localization of the 4*f* states in the coarse of lanthanide contraction, but mainly to a respective effect on the 6*s* derived bands that reveal in Yb less *d* admixtures than in Ce and are, thus, less suitable for hybridization with 4*f* states. On the other hand, splittings and dispersions of the 4*f* states have been observed at the $\bar{\Gamma}$ point that are obviously caused by hybridization of the Yb 4*f* states with W 5*d*-derived bands. Since the lattices of the Yb overlayer and the substrate are incoherent to each other, the phe-

nomena do not reflect properties of a Yb 4*f*-derived band but the effects of a **k**-dependent interaction of Yb impurities with W 5*d*-derived bands.

Acknowledgements

This work was funded by the Deutsche Forschungsgemeinschaft, SFB 463, Projects B4 and B16 and by the Science and Technology Center in Ukraine (STCU), Project 4930. We would like to acknowledge BESSY staff for technical support during experiment.

References

[1] E. Weschke et al., Phys. Rev. Lett. 83 (1999) 584.
[2] F. Patthey et al., Phys. Rev. B 42 (1990) 8864.
[3] D. Malterre, M. Grioni, Y. Baer, Adv. Phys. 45 (1996) 299.
[4] D.V. Vyalikh et al., Phys. Rev. Lett. 96 (2006) 026404.
[5] Ping Sun, Gabriel Kotliar, Phys. Rev. Lett. 91 (2003) 037209.
[6] Kristjan Haule, Viktor Oudovenko, Sergej Y. Savrasov, Gabriel Kotliar, Phys. Rev. Lett. 94 (2005) 036401.
[7] Lorenzo De Leo, Marcello Civelli, Gabriel Kotliar, Phys. Rev. B 77 (2008) 075107.
[8] R. Hayn, Y. Kucherenko, J.J. Hinarejos, S.L. Molodtsov, C. Laubschat, Phys. Rev. B 96 (2001) 115106.
[9] S. Danzenbächer et al., Phys. Rev. Lett. 96 (2006) 106402.
[10] M. Posternak, H. Krakauer, A.J. Freeman, D.D. Koelling, Phys. Rev. B 21 (1980) 5601.
[11] F. Gerken, A.S. Flodström, J. Barth, L.I. Johansson, C. Kunz, Phys. Scr. 32 (1985) 43.
[12] N. Mårtensson, A. Stenborg, Q. Björneholm, A. Nilsson, J.N. Andersen, Phys. Rev. Lett. 60 (1988) 1731.
[13] M. Bodenbach, A. Höhr, C. Laubschat, G. Kaindl, M. Methfessel, Phys. Rev. B 50 (1994) 14446.
[14] W.D. Schneider, C. Laubschat, B. Reihl, Phys. Rev. B 27 (1983) 6538.
[15] M. Domke, T. Mandel, C. Laubschat, M. Prietsch, G. Kaindl, Surf. Sci. 189–190 (1987) 268.
[16] C. Laubschat, W. Grentz, G. Kaindl, Phys. Rev. B 36 (1987) 8233.
[17] B. Johansson, N. Mårtenson, Phys. Rev. B 21 (1980) 4427.
[18] A.R. Miedema, J. Less Common Met. 46 (1976) 67.
[19] G. Kaindl et al., Phys. Rev. B 51 (1995) 7920.
[20] O.K. Andersen, Phys. Rev. B 12 (1975) 3060.
[21] A.R. Mackintosh, O.K. Andersen, in: M. Springford (Ed.), Electrons in the Fermi Surface, Cambridge University Press, New York, 1980.
[22] H.L. Skriver, The LMTO Method, Springer, New York, 1984.
[23] O.K. Andersen, in: P. Phariseau, W. Temmerman (Eds.), The Electronic Structure of Complex Systems, Plenum, New York, 1984.
[24] O.K. Andersen, Z. Pawlowska, O. Jepsen, Phys. Rev. B 34 (1986) 5253.
[25] J.C. Slater, The self-consistent-field method for crystal, in: P.M. Marcus, J.F. Janak, A.R. Williams (Eds.), Computational Methods in Band Theory, Plenum Press, New York, 1971.
[26] F. Schiller, M. Heber, V.D. Servedio, C. Laubschat, Phys. Rev. B 68 (2003) 233103.
[27] Yu. Kucherenko et al., Phys. Rev. B 70 (2004) 045105.